Received 9 February 2022
Revised 28 February 2022
Accepted 29 March 2022

A vertical coupling dynamic analysis method and engineering application of vehicle–track–substructure based on forced vibration

Guolong Li, Mangmang Gao, Jingjing Yang and Yunlu Wang
Infrastructure Inspection Research Institute, China Academy of Railway Sciences Corporation Limited, Beijing, China, and
Xueming Cao
Standards and Metrology Research Institute, China Academy of Railway Sciences Corporation Limited, Beijing, China

Abstract

Purpose – This study aims to propose a vertical coupling dynamic analysis method of vehicle–track–substructure based on forced vibration and use this method to analyze the influence on the dynamic response of track and vehicle caused by local fastener failure.

Design/methodology/approach – The track and substructure are decomposed into the rail subsystem and substructure subsystem, in which the rail subsystem is composed of two layers of nodes corresponding to the upper rail and the lower fastener. The rail is treated as a continuous beam with elastic discrete point supports, and spring-damping elements are used to simulate the constraints between rail and fastener. Forced displacement and forced velocity are used to deal with the effect of the substructure on the rail system, while the external load is used to deal with the reverse effect. The fastener failure is simulated with the methods that cancel the forced vibration transmission, namely take no account of the substructure–rail interaction at that position.

Findings – The dynamic characteristics of the infrastructure with local diseases can be accurately calculated by using the proposed method. Local fastener failure will slightly affect the vibration of substructure and carbody, but it will significantly intensify the vibration response between wheel and rail. The maximum vertical displacement and the maximum vertical vibration acceleration of rail is 2.94 times and 2.97 times the normal value, respectively, under the train speed of 350 $km \cdot h^{-1}$. At the same time, the maximum wheel–rail force and wheel load reduction rate increase by 22.0 and 50.2%, respectively, from the normal value.

Originality/value – This method can better reveal the local vibration conditions of the rail and easily simulate the influence of various defects on the dynamic response of the coupling system.

Keywords Vehicle–track–substructure, Coupling dynamic analysis, Forced vibration, Vibration response, Fastener, Failure

Paper type Research paper

The study was funded by the Research Fund of Shanghai Bureau Group Corporation (2021142); Science Foundation of China State Railway Group Corporation Limited (P2021T013) and Science Foundation of China Academy of Railway Sciences Corporation Limited (2021YJ250).

Railway Sciences
Vol. 1 No. 2, 2022
pp. 224-240
Emerald Publishing Limited
e-ISSN: 2755-0915
p-ISSN: 2755-0907
DOI 10.1108/RS-04-2022-0016

1. Introduction

High-speed railways have been in service for more than ten years in China. The large traffic volume, high speed and long-term operation put the infrastructure in the service status different from that in the early period upon the completion. Defects have occurred such as deteriorated track conditions caused by creep camber of bridges (Li, Yang, & Ma, 2020; Tian, Gao, Liu, & Cai, 2020a), gaps between track slabs and mortar layers (Li & Shi, 2019; Zhao & Liu, 2019) caused by thermal deformation (Tian, Gao, Yang, *et al.*, 2020b) of track slabs, continuous development of settlement (Zhang, Shan, & Yang, 2017) exceeding the limits specified in relevant standards, great thermal deformation of large-span bridges (Niu, Wang, & Tang, 2020) and beam-end expansion devices in poor working condition. The needs for defect mechanism analysis, dynamic performance evaluation and formulation of evaluation standards are more and more urgent. The conventional vehicle–track–bridge dynamic analysis model focuses more on the dynamic performance evaluation at the design stage, and it is difficult for the model to accurately simulate the parameter changes of local tracks or substructures. Therefore, a more accurate and efficient dynamic analysis model should be built in light of track structures, and the vehicle–track–bridge dynamic analysis algorithm should be modified accordingly.

In the track dynamic analysis model, rails are the links between vehicles and tracks, and they are directly related to the calculation efficiency and accuracy. On the basis of analyzing the conventional track model and its limitations, the present paper puts forward an optimized track structure treatment solution and a vehicle–track–substructure dynamic analysis method and uniformly treats infrastructure such as subgrade, bridges and tunnels as substructures. In this way, local defects can be accurately simulated and the dynamic analysis of various combined structures of infrastructure is simplified.

1.1 Conventional track structure model and its limitations

Most of the early vehicle–bridge vibration studies focus on bridges, without considering (or just simply considering) the vibration influence of the track structure. Usually, the whole rail-sleeper-track bed mass system is applied to the beam body as a secondary dead load. The wheel–rail interaction is calculated by taking the sum of beam displacement and random track irregularity as the rail displacement. While various ballastless track structures are widely used, the follow-up relationship between the track and the bridge deck is greatly affected by the track structure, and the track structure vibration should not be neglected.

Chen, Lei and Fang (2011), Zhu, Gong, Zhang, Yu and Cai (2018) built a rail-bridge integrated model with the finite element method and solved the dynamic response of rail and bridge with the direct stiffness method. Bridges are significantly different from tracks in terms of material, mass and stiffness, and the unit dimensions and track layout need to be coordinated with each other. Therefore, the modeling is more difficult than separate track modeling and bridge modeling. Besides, the track and bridge integration will lead to a significant increase in the solution scale of the structure, and this will affect the calculation efficiency to a certain extent.

At present, separate track-bridge model is more common. The slab ballastless track is taken as an example. Figure 1 shows the side view of a typical slab track dynamic model

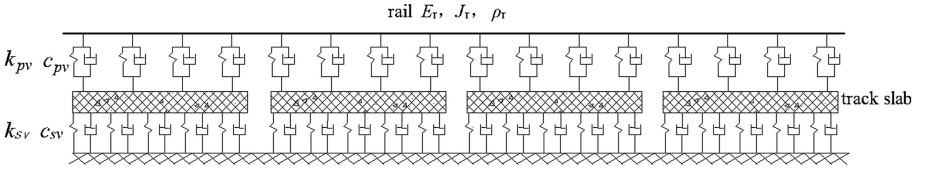

Figure 1.
Slab track dynamic model

(the bridge structure is not drawn for the convenience of illustration) where E_r is the elastic modulus of rail material; J_r is the bending moment of inertia of rail section; ρ_r is the unit weight of rail material; k_{pv} and c_{pv} are the stiffness and damping of the rail pad, respectively; and k_{sv} and c_{sv} are the stiffness and damping of the cement asphalt (CA) mortar, respectively.

The slab track is composed of rails, fasteners, track slabs, bollards, CA mortar and concrete bases. The track vibration mainly includes rail vibration and track slab vibration. The rail pad provides elasticity between the rail and the track slab and the CA mortar provides elasticity between the track slab and the concrete base. Both the left and right rails are regarded as infinitely long Euler beams supported by discrete elastic points. After considering the influence of the boundary conditions of rail vibration, Pan and Gao (2008), Zhai (2015), Zhang, Tan and Wu (2012) took the rail and the substructure in the track model into separate considerations. The infinitely long Euler beam model of the rail was simplified to a finitely long simply supported beam model, the canonical coordinates of the rail were introduced and the vibration mode superposition method was adopted to establish the rail motion equation (Xu, Li, Wu, & Chen, 2010; Yang & Hwang, 2016). The train load and the rail pad support are external loads applied onto the simply supported beam. The mechanical model and load state of the rail are shown in Figure 2 where x_0 is the distance between the last wheelset of the vehicle and the rail end; l is half of the length between bogie centers; l_1 is half of the wheelbase; F_{p1}, F_{p2}, F_{p3} and F_{p4} are wheel–rail vertical force applied by vehicles on rails; F_{rs1}, F_{rs2}, F_{rsi} and F_{rsn} are vertical forces applied by the substructure on rails; z_r is the vertical displacement of rail; L is the calculated length of rail; x_i ($i = 1, 2, \ldots, n$) is the x-coordinate of each fastener and v is the train speed.

In the process of actual vibration, the support force of the rail at the fastener position increases with the increase of the loads. However, in the dynamic analysis, the displacement calculation needs definite loads, and so the actual calculation process is as follows.

(1) Calculate the rail displacement under the wheel–rail vertical force;

(2) Calculate the support reaction force at each fastener position based on the rail displacement obtained above;

(3) Calculate the rail displacement under both the support reaction force and the wheel–rail force;

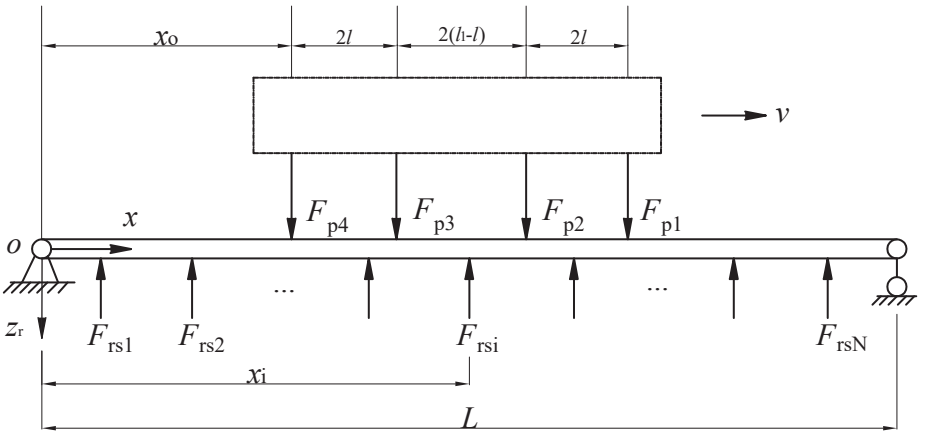

Figure 2.
Loads on rails in conventional track and bridge structure

(4) If the difference between the rail displacement this time and the rail displacement used to calculate the wheel–rail force exceeds the allowable error, the wheel–rail force should be calculated again;

(5) Repeat steps (1)–(4) until the difference between the results of two consecutive rail displacement calculations meets the iteration accuracy.

The calculation accuracy of the rail dynamic analysis model above is affected by the calculated length. When the calculated length is greater and if the rail is treated as a simply supported beam, repeated instability of the rail displacement will occur. Through theoretical deduction, if the influence of inertia force and damping force is not considered, only the static force is considered; the convergence of the calculation results requires that the support stiffness provided by the rail pad should not be greater than 2 times the stiffness provided by the rail as a simply supported beam. After canonical coordinates are introduced, this contradiction can be solved by limiting the order of the cutoff mode, but in this way, the local high-frequency vibration of the rail cannot be revealed (Li, 2018), and the rail dynamic analysis results are smaller than the real values.

2. Optimized track structure model and its characteristics

In order to simulate local track defects and avoid the possible calculation divergence caused by treating the rail as a simply supported beam, it is necessary to build a three-dimensional finite element model of the rail subsystem and the substructure subsystem and calculate the dynamic response by using the direct stiffness method. However, in order to make the modeling easier and the solution scale smaller, it is necessary to properly separate the track–bridge structure. Figure 3 shows the optimized vertical coupling dynamic model of the track system and the substructure.

A spring-damping unit is used to simulate the rail pad. The rail subsystem composed of rails and fasteners and the substructure subsystem composed of track slabs, bridges and tunnels are processed separately. The train load is the external load on the rail subsystem, but the track slab action is applied on the rail subsystem in the form of forced displacement and forced velocity at the fasteners. In this way, vibration conditions of the rails and the substructures can be better separately revealed, and the possible nonconvergence caused by using force boundary conditions to simulate the constraint of the rail pad on the rail is avoided. Moreover, the substructure model and the rail subsystem model are independent and thus can be easily adapted to a variety of track types and special cases, such as separation of track slabs, fastener failures, transition sections, bridges and tunnels. The mechanical model and loads conditions of rails in this case are shown in Figure 4 where z_{si} and v_{si} are the vertical displacement and the vertical velocity at each fastener position of track slabs, respectively.

3. Vehicle, rail system, substructure models and their motion equations

When the optimized track structure is adopted, the vehicle–track–substructure coupling system includes three subsystems: vehicle subsystem, rail subsystem and substructure subsystem. A vehicle model is built based on the multi-rigid body theory, and a rail

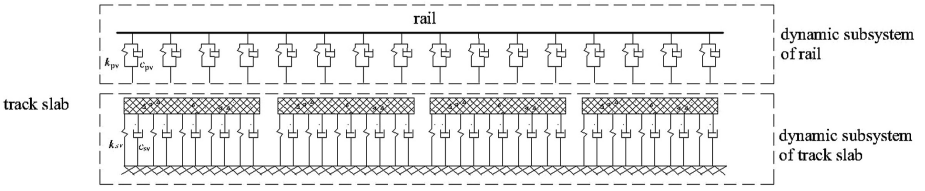

Figure 3.
Vertical coupling dynamic model of track system and substructure

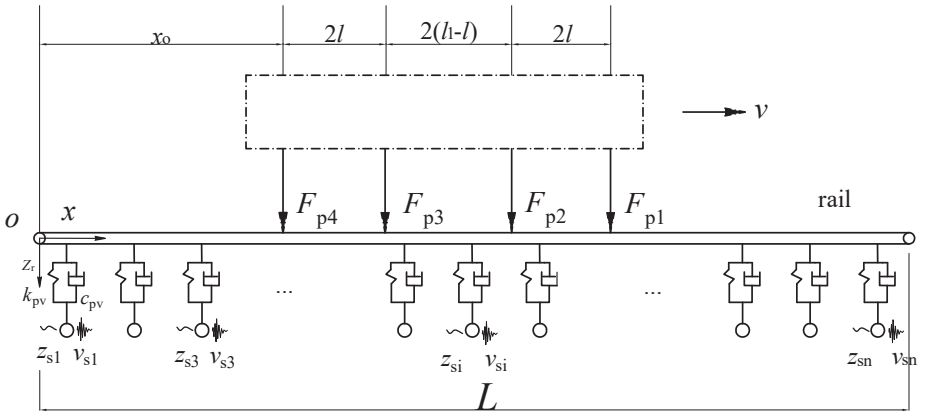

Figure 4.
Loads on rails in optimized track and bridge structure

subsystem model and substructure subsystem model are built based on the finite element. The action of the substructure is applied on the rail subsystem in the form of forced displacement and forced velocity at the fasteners, while the action of the rail subsystem is applied on the substructure in the form of load. The direct stiffness method is adopted to solve the dynamic response of each subsystem.

3.1 Vehicle model and motion equation

The train consists of multiple cars and each car consists of one carbody, two bogies and four wheelsets. Taking the passenger train with secondary suspension as an example, in consideration of the vertical vibration of the train, each car involves ten degrees of independent freedom, including bouncing and pitching of the carbody and frame as well as bouncing of the wheelsets. The vehicle dynamic analysis model is shown in Figure 5, and the physical meaning of each variable is shown in Table 1.

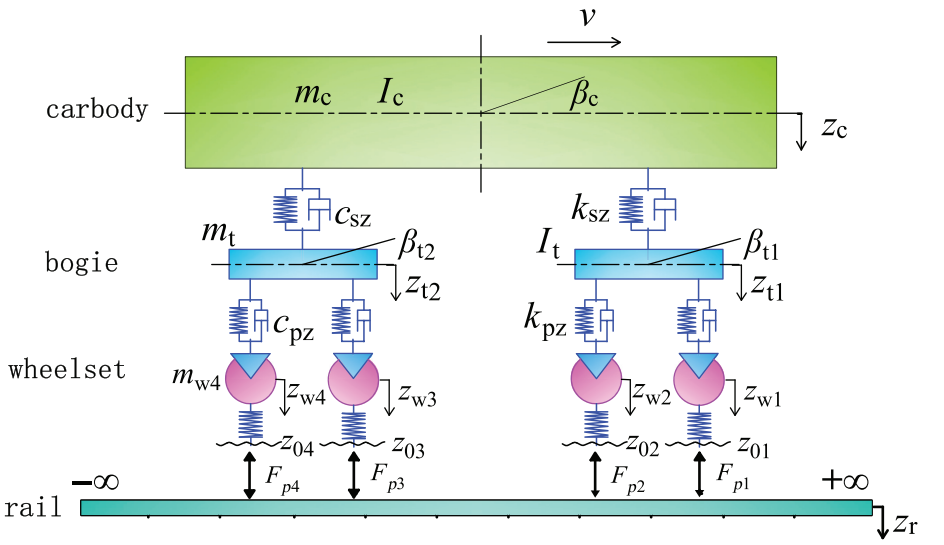

Figure 5.
Vehicle dynamic analysis model

Variable	Symbol	Variable	Symbol	Variable	Symbol
Mass of carbody	m_c	Bouncing displacement of carbody	z_c	Pitching displacement of bogie	β_{t1}, β_{t1}
Mass of bogie	m_t	Bouncing displacement of bogie	z_{t1}, z_{t2}	Primary vertical stiffness	k_{pz}
Mass of wheelset	m_w	Bouncing displacement of wheelset	z_{w1}, z_{w2}, z_{w3}, z_{w4}	Primary vertical damping	c_{pz}
Pitching rotational inertia of carbody	I_c	Geometric irregularity of track	Z_{01}, z_{02}, z_{03}, z_{04}	Secondary vertical stiffness	k_{sz}
Pitching rotational inertia of bogie	I_t	Pitching displacement of carbody	β_c	Secondary vertical damping	c_{sz}

Table 1. Physical meaning of each variable in the vehicle model

Assuming that the displacement vector of the vehicle is X_v, the velocity vector is $\dot{X}_v$ and the acceleration vector is $\ddot{X}_v$, the vehicle motion equation is established according to the multi-rigid body theory and the D' Alembert principle as follows:

$$M_v\ddot{X}_v + C_v\dot{X}_v + K_vX_v = F_v \tag{1}$$

where M_v, C_v and K_v are the mass matrix, damping matrix and stiffness matrix of the vehicle, respectively; F_v is the load vector acting on each degree of freedom of the vehicle during the vibration.

The compositions of mass, damping and stiffness matrixes are as follows:

$$M_v = diag(m_c\ I_c\ m_t\ I_t\ m_t\ I_t\ m_w\ m_w\ m_w\ m_w) \tag{2}$$

$$\boldsymbol{K}_v = \begin{pmatrix} 2k_{sz} & & & & & & & & & \\ & 2l^2k_{sz} & & & & & & & & \\ -k_{sz} & lk_{sz} & k_{sz}+2k_{pz} & & & \text{Symmetrical} & & & & \\ & & & 2l_1k_{pz} & & & & & & \\ -k_{sz} & -lk_{sz} & & & k_{sz}+2k_{pz} & & & & & \\ & & & & & 2l_1k_{pz} & & & & \\ & & -k_{pz} & l_1k_{pz} & & & k_{pz} & & & \\ & & -k_{pz} & -l_1k_{pz} & & & & k_{pz} & & \\ & & & & -k_{pz} & l_1k_{pz} & & & k_{pz} & \\ & & & & -k_{pz} & -l_1k_{pz} & & & & k_{pz} \end{pmatrix} \tag{3}$$

$$X_v = (z_c, \beta_c, z_{t1}, \beta_{t1}, z_{t2}, \beta_{t2}, z_{w1}, z_{w2}, z_{w3}, z_{w4}) \tag{4}$$

$$X_v = (0, 0, 0, 0, 0, 0, F_{p1}-F_0, F_{p2}-F_0, F_{p3}-F_0, F_{p4}-F_0) \tag{5}$$

where F_0 is the average static axle load of the wheelsets.

The damping matrix C_v and the stiffness matrix K_v are similar and so not repeated.

3.2 Dynamic analysis models and motion equations of rail and substructure

As shown in Figure 3, a rail subsystem model is built by using the nodes in an upper layer and a lower layer corresponding to each other. The rail is a continuous Euler beam with elastic discrete point support. The nodes in the lower layer represent fasteners. The elastic constraint of the rail pad is expressed by the spring-damping unit between the upper and lower nodes.

Assuming that the displacement vector of the rail subsystem is X_r, the velocity vector is $\dot{X}_r$ and the acceleration vector is $\ddot{X}_r$, the dynamic equilibrium equation of the rail can be obtained from the rail stiffness matrix, mass matrix and load vector as follows.

$$M_r\ddot{X}_r + C_r\dot{X}_r + K_rX_r = F_r \tag{6}$$

where M_r, C_r and K_r are the mass matrix, damping matrix and stiffness matrix of the rail, respectively; F_r is the load vector acting on each degree of freedom of the rail during the vibration.

The substructure model can simulate such structures as ballasted or ballastless tracks, subgrade, bridges and tunnels by using slab unit, beam unit, spring-damping unit, etc. Assuming that the displacement vector of the substructure is X_b, the velocity vector is $\dot{X}_b$ and the acceleration vector is $\ddot{X}_b$, the motion equation of the substructure can be written in a matrix form as follows:

$$M_b\ddot{X}_b + C_b\dot{X}_b + K_bX_b = F_b \tag{7}$$

where M_b, C_b *and* K_b are the mass matrix, damping matrix and stiffness matrix of the substructure, respectively; F_b is the generalized load vector of the substructure.

3.3 Vehicle–track–substructure coupling equation and analysis method

After the dynamic equilibrium equations of vehicle, rail and substructure are established, the entire vehicle–track–substructure system is decomposed into three subsystems and two coupling systems of action interfaces. The vehicle–rail interaction is expressed by wheel–rail force. The rail–substructure interaction is expressed by forced displacement and forced velocity at the fasteners applied by track slabs onto the rails. At the same time, the rails counteract on the track slabs with spring force and damping force at the fasteners. The three subsystems are coupled through force equilibrium conditions and deformation coordination conditions. The motion equation of the coupling system can be expressed as follows:

$$M\ddot{X} + C\dot{X} + KX = F \tag{8}$$

In which,

$$M = \begin{pmatrix} M_v & 0 & 0 \\ 0 & M_r & 0 \\ 0 & 0 & M_b \end{pmatrix}$$

$$C = \begin{pmatrix} C_{vv} & C_{vr} & 0 \\ C_{rv} & C_{rr} & C_{rb} \\ 0 & C_{br} & C_{bb} \end{pmatrix}$$

$$K = \begin{pmatrix} K_{vv} & K_{vr} & 0 \\ K_{rv} & K_{rr} & K_{rb} \\ 0 & K_{br} & K_{bb} \end{pmatrix}$$

$$X = (X_v,\ X_r,\ X_b)^T$$

$$F = (F_v,\ F_r,\ F_b)^T$$

where X, $\dot{X}$, $\ddot{X}$, F are the displacement, velocity, acceleration and load column vectors of the coupling system, respectively; M, C and K are the mass matrix, damping matrix and stiffness matrix of the coupling system, respectively.

To determine the wheel–rail force, the Hertz nonlinear elastic contact theory is adopted, and wheels up off the rail, i.e. jumping on the rail, is allowed. The influence of track geometric irregularity is considered when the wheel–rail force is calculated.

When the substructure's action on the rail subsystem is calculated, for the forced vibration at fasteners, the common method of "replacing main elements with 1 and other elements with 0" (Wang, 2004) is used to process the stiffness matrix and the damping matrix of the rail subsystem. Because the rail pad is regarded as a massless spring-damping unit in the model, the influence of the vibration acceleration of the substructure on the rail subsystem is not considered; the rail subsystem's action on the substructure is directly calculated according to the relative displacement and relative velocity between the rail and the track slab.

After the dynamic equations of vehicle, track and substructure are determined, the Newmark-β method is used for solution. Because the interaction between each subsystem at each time step is related to the system response at that time, iteration is necessary. Force equilibrium conditions are used to calculate the interaction between the subsystems. Therefore, the convergence is conditioned on that displacement difference of vehicle, rail and substructure between two consecutive iterations at each time step meets the accuracy requirement, and the displacement accuracy limit selected is 0.1 μm. The calculation process is shown in Figure 6.

4. Model verification

In order to verify the correctness and applicability of the method, a model of the subgrade +10-span 32 m simply supported beam bridge + subgrade track–bridge structure is built. The track is ballastless. The finite element model of the 10-span 32 m simply supported beam bridge is shown in Figure 7 and that of the bridge track in Figure 8. In order to fully consider the influence of the random irregularity of the track and the creep upwarp of the bridge, the measured static elevation data of the track shown in Figure 9 is used as the input irregularity. The peak value of the track longitudinal level caused by the creep upwarp of the bridge is up to 5.02 mm. The train is a CRH380A high-speed comprehensive inspection train of China, with a running speed of 300 $km \cdot h^{-1}$. In consideration of the influence of the bridge entry/exit length and the vehicle length, the total length of the model is 1,000 m. Vehicle–track–bridge dynamic simulation analysis is conducted.

The measured vertical vibration acceleration of the carbody, and the simulation analysis results are given in Figure 10. The measured maximum vertical vibration acceleration of the carbody is 0.540 $m \cdot s^{-2}$, and the calculated value is 0.566 $m \cdot s^{-2}$. The measured value conforms with the calculated value.

The vertical displacement time history curves of subgrade section and bridge midspan obtained from simulation analyses are given in Figure 11. It can be seen from Figure 11 that the maximum vertical displacement of the rail on the subgrade section, that of the rail on the bridge midspan and that of the bridge are 0.825, 1.248 and 0.440 mm respectively. The calculated results conform with the data measured in integrated commissioning and test on a high-speed railway in China.

According to the comparison between the analysis results and the measured data, the present model can fully reveal the vibration response of vehicles, tracks and bridges, and its calculation accuracy meets the requirements of engineering application.

5. Application

The present vehicle–track–substructure dynamic analysis model can take into account the influence of local defects of infrastructure, such as tracks and bridges, on the dynamic response of the system. Taking fastener failures as an example, a 100 m-long CRTS I

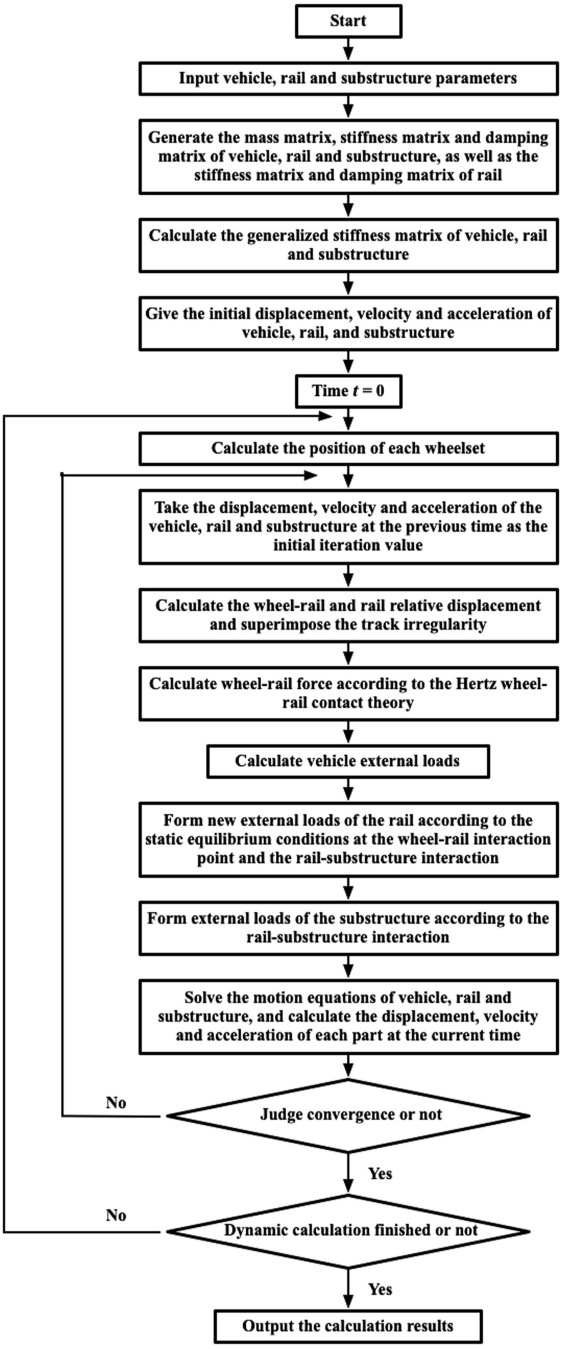

Figure 6.
Dynamic analysis process

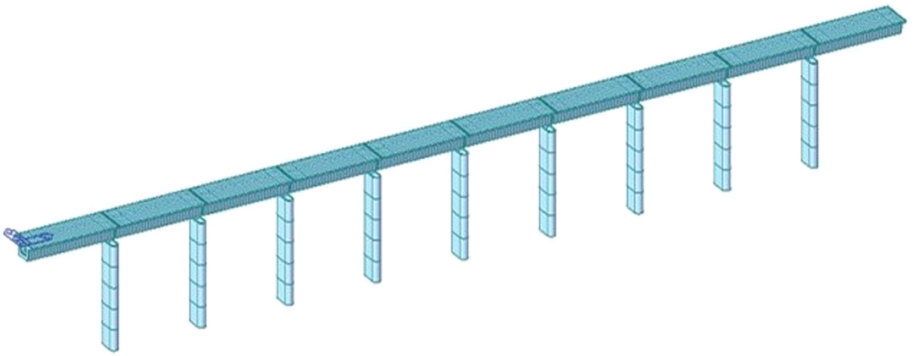

Figure 7.
Finite element model of 10-span 32 m simply supported beam bridge

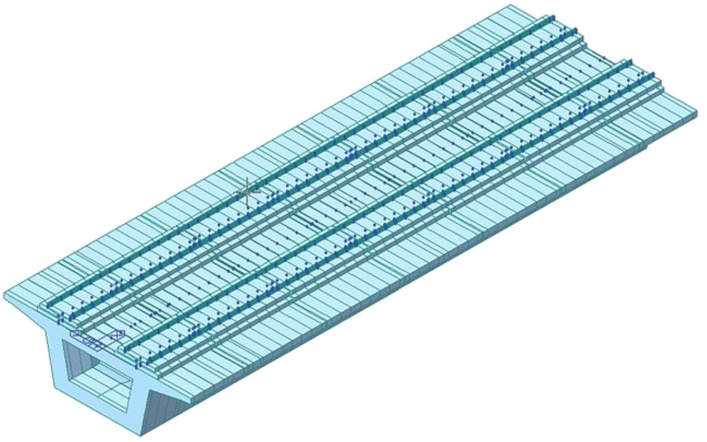

Figure 8.
Finite element model of bridge track

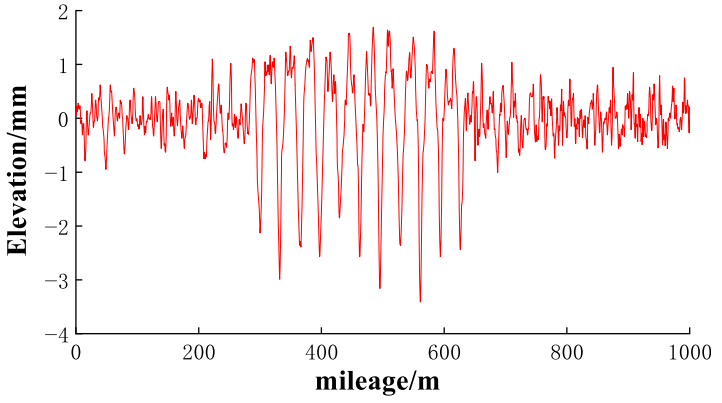

Figure 9.
Measured static elevation data of track

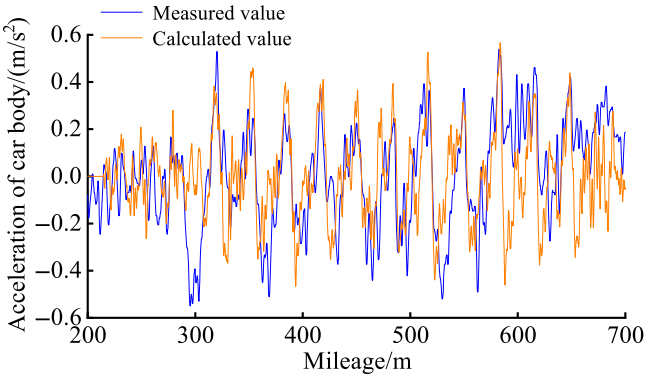

Figure 10.
Vertical vibration acceleration of carbody

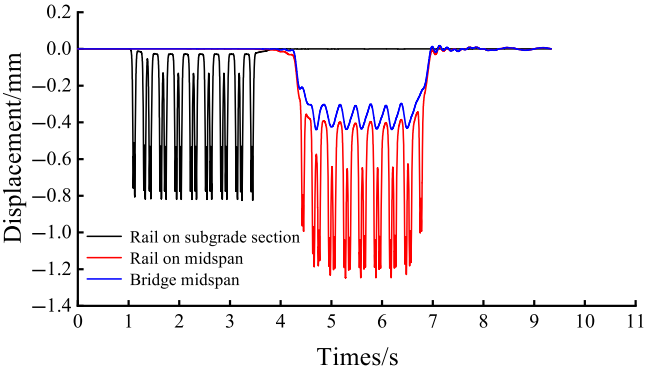

Figure 11.
Vertical displacement of rails and bridge

ballastless slab track is analyzed. In consideration of the boundary effect, train length and operation stability, the total length of the ballastless track is 700 m, as shown in Figure 12.

In light of the results of the field investigation, the case of the failure of two consecutive fasteners at 352.836 m and 353.465 m in the middle of the track is selected. Refer to Figure 13

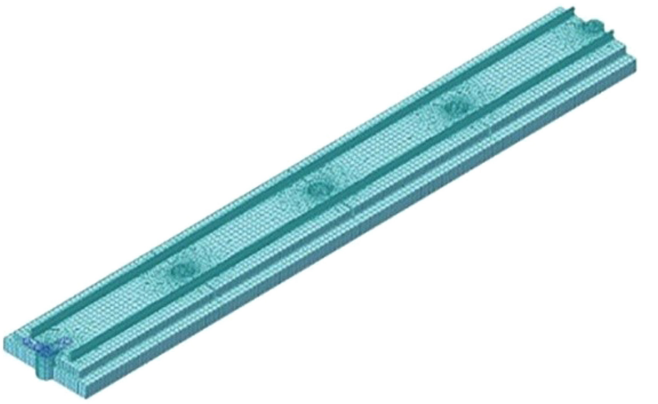

Figure 12.
Local ballastless track finite element model

for details. The dynamic response comparison and simulation analyses of vehicle, rail and track slab in the case of fastener failure and the case of normal service of fasteners are carried out.

The fastener failure may be simulated with two methods: (1) assign the stiffness and damping provided by the corresponding fastener to 0 and (2) cancel the forced vibration transmission, namely take no account of the substructure–rail interaction at that position. This paper adopts the second method. In the model, the vertical static stiffness of the elastic cushion under rail is 25 $MN \cdot m^{-1}$, and the damping is 70 $kN \cdot s \cdot m^{-1}$. The train consists of four motor cars and four trailer cars, and the calculated speed is 300, 320, 340, 350 and 385 $km \cdot h^{-1}$, respectively. The irregularities selected are shown in Figure 14.

Table 2 gives the maximum dynamic response of the vehicle and rails and track slabs at 352.836 m and 353.465 m in the case of fastener failure and the case of normal service of fasteners. Figures 15–19 show the rail displacement, vibration acceleration, wheelset vibration acceleration and wheel–rail force time history curves at 352.836 m and 353.465 m with the speed of 350 $km \cdot h^{-1}$.

The analysis results show that due to the wheel–rail contact and the secondary suspension characteristics of the vehicle, the fastener failure has a small impact on the riding comfort and the substructure but has a great impact on the rail vibration. The wheel–rail vibration increases. The wheel–rail force and the rate of wheel load reduction increase significantly. When fasteners are in normal service, the maximum vertical vibration acceleration of the wheelset at a speed of 350 $km \cdot h^{-1}$ is 35.652 $m \cdot s^{-2}$, the maximum vertical displacement of the rail is 0.943 mm, the maximum vertical acceleration of the rail is 66.20 $m \cdot s^{-2}$, the maximum wheel-rail vertical force is 85.951 kN and the maximum rate of wheel load reduction is 0.265. When fasteners fail, the maximum vertical vibration acceleration of the wheelset is 46.266 $m \cdot s^{-2}$, the maximum vertical displacement of the rail is 2.777 mm which is 2.94 times the normal value, the maximum vertical acceleration of the rail is 196.638 $m \cdot s^{-2}$ which is 2.97 times the normal value, the maximum wheel–rail force is 104.872 kN

Figure 13.
Map of fastener failures

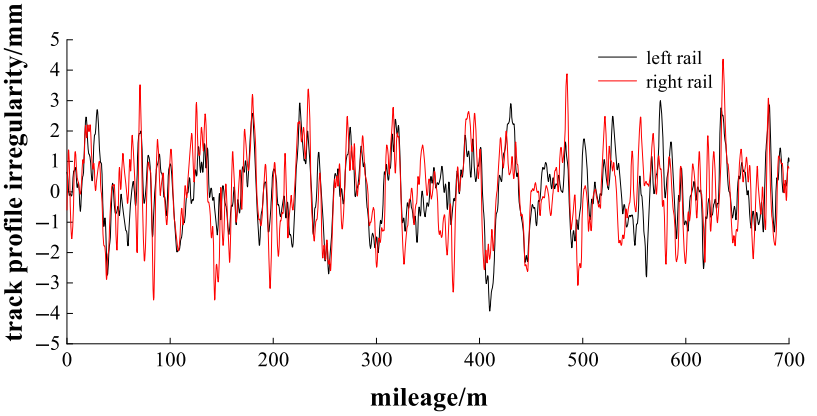

Figure 14.
Track geometric irregularity on subgrade section of high-speed railway

Table 2.
Maximum vehicle and track dynamic response

Case	Speed/(km·h^{-1})	Vertical vibration acceleration of carbody/ (m·s^{-2})	Vertical vibration acceleration of wheelset/ (m·s^{-2})	Vertical displacement of rail/(mm)	Vertical vibration acceleration of rail/ (m·s^{-2})	Vertical displacement of track slab/mm	Vertical vibration acceleration of track slab/ (m·s^{-2})	Wheel-rail force/kN	Rate of wheel load reduction
Normal service of fasteners	300	0.184	27.485	0.937	54.033	0.034	5.343	81.594	0.178
	320	0.183	31.000	0.939	59.208	0.035	6.567	82.379	0.194
	340	0.179	34.941	0.942	63.388	0.036	8.807	84.526	0.236
	350	0.177	35.652	0.943	66.200	0.037	9.518	85.591	0.230
	385	0.180	43.454	0.945	82.299	0.041	16.093	90.538	0.265
Fastener failure	300	0.184	38.765	2.700	144.147	0.043	6.322	98.829	0.377
	320	0.185	42.350	2.721	167.048	0.044	7.728	100.916	0.385
	340	0.180	45.468	2.765	185.473	0.046	11.086	104.167	0.389
	350	0.179	46.266	2.777	196.638	0.047	12.329	104.872	0.398
	385	0.182	54.435	2.800	229.436	0.049	16.320	108.163	0.453

which is 22.0% higher than that in case of normal service and the maximum rate of wheel load reduction is 0.398 which is 50.2% higher than that in case of normal service.

Under the action of the train load, local fastener failures will increase the vertical displacement of the rails in this area, damage the rails and fasteners near this area more severely and may affect the train operation safety in worse cases.

6. Conclusion

The rail and the substructure are treated as two separate subsystems, and a finite element model is built for each of the subsystems. The substructure subsystem considers the infrastructure, such as subgrade, bridges and tunnels. The rail subsystem adopts nodes in two layers. The rail in the upper layer is regarded as a continuous beam supported by elastic

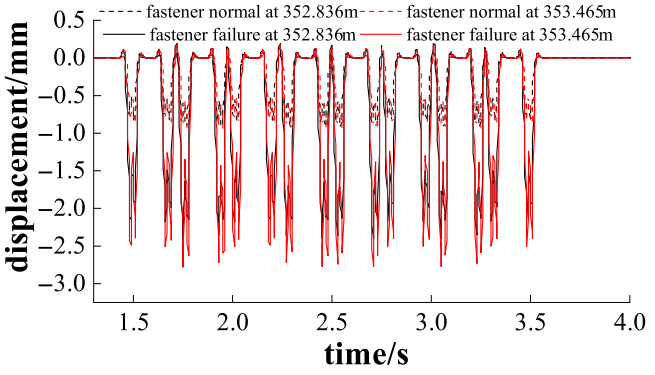

Figure 15.
Time history curve of rail vertical displacement in case of fastener failure and normal service at a speed of 350 km·h^{-1}

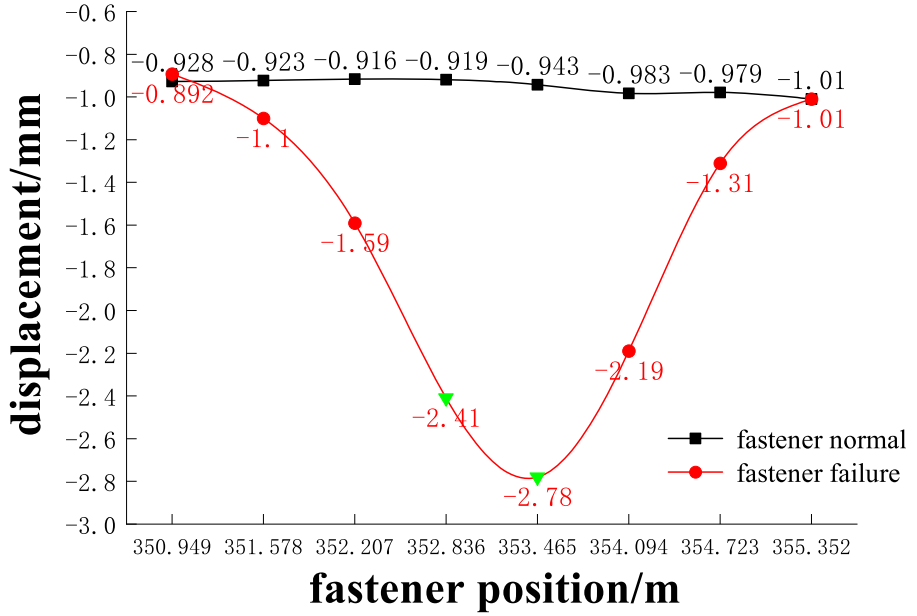

Figure 16.
Rail vertical displacement at different fasteners in case of fastener failure and normal service at a speed of 350 km·h^{-1}

discrete points. The nodes in the lower layer represent fasteners. The rail and fasteners are connected in the form of a spring-damping unit. On this basis, the action of the substructure on the rail is processed with the forced displacement and forced velocity method. This method

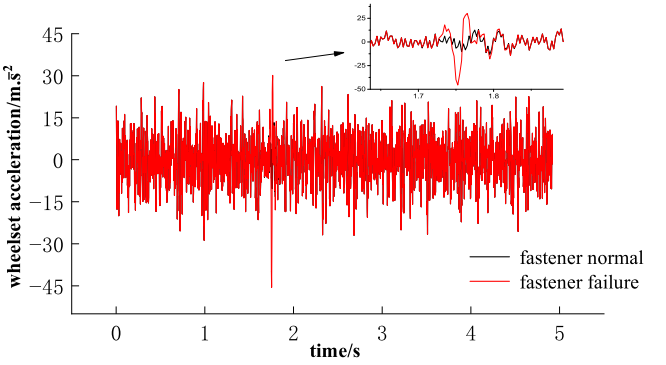

Figure 17.
Time history curve of wheelset vertical vibration acceleration in case of fastener failure and normal service at a speed of 350 km·h^{-1}

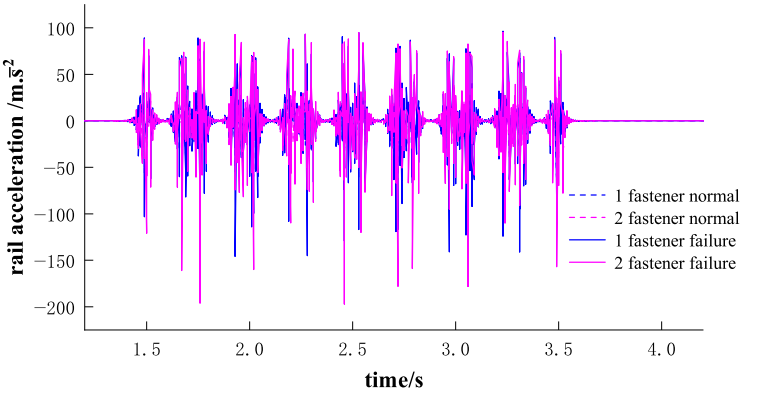

Figure 18.
Time history curve of rail vertical vibration acceleration in case of fastener failure and normal service at as speed of 350 km·h^{-1}

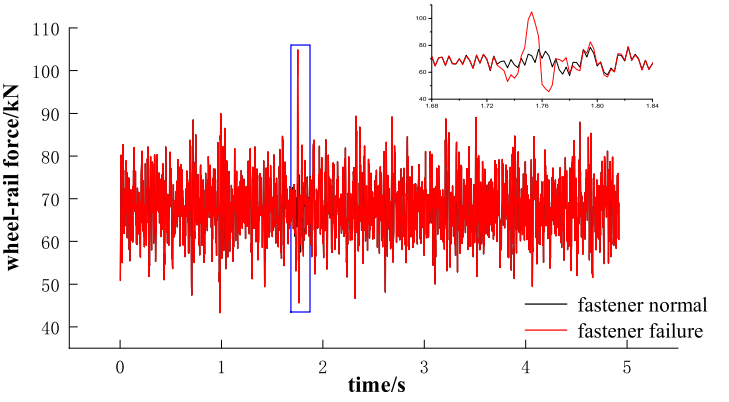

Figure 19.
Time history curve of wheel-rail vertical force in case of fastener failure and normal service at a speed of 350 km·h^{-1}

can better reveal the local vibration conditions of the rail and easily simulate the influence of various defects on the dynamic response of the coupling system.

The present model is used to analyze the vehicle–track–substructure dynamic response in the case of local fastener failures. The result shows that the loss of fasteners will cause local high-frequency vibration between wheel and rail; at a speed of 350 $km \cdot h^{-1}$, the maximum vertical displacement of the rail is 2.94 times the normal value, the maximum vertical acceleration of the rail is 2.97 times the normal value, the maximum wheel-rail force is 22.0% higher than the normal value and the maximum rate of wheel load reduction is 50.2% higher than the normal value.

References

Chen, S., Lei, X., & Fang, J. (2011). Vibration characteristics of the passenger line bridge vertical coupling system. *Journal of East China Jiaotong University*, *28*(5), 41–45.

Li, D., & Shi, C. (2019). Effect of interfacial cracks of mortar layer of CRTS II slab ballastless track on stress of longitudinal reinforcing bars between track slabs. *China Railway Science*, *40*(5), 22–27.

Li, D., Yang, F., & Ma, H. (2020). Effect of periodic track irregularities on simply supported beam bridge with common span for high-speed railway. *China Railway Science*, *41*(3), 59–67.

Li, G. (2018). *Optimization Research on the Vehicle-track Vertical Coupling Interaction of High Speed Railway*. Beijing: China Academy of Railway Sciences.

Niu, Y., Wang, Y., & Tang, Y. (2020). Analysis of temperature-induced deformation and stress distribution of long-span concrete truss combination arch bridge based on bridge health monitoring data and finite element simulation. *International Journal of Distributed Sensor Networks*, *16*(10). doi: 10.1177/1550147720945205.

Pan, J., & Gao, M. (2008). *Dynamic Analysis of Railway Vehicle-track-bridge System*. Beijing: China Railway Publishing House.

Tian, X., Gao, L., Liu, M., & Cai, X. (2020a). Study on residual creep arching threshold of 32 m simply-supported beam bridge of high speed railway after track laying. *China Railway Science*, *41*(3), 45–59.

Tian, X., Gao, L., Yang, F., Sun, X., Wei, H., & Sun, J. (2020b). Management standard for cyclic irregularity of ballastless track slab based on dynamic short chord. *China Railway Science*, *41*(6), 30–38.

Wang, D. (2004). *Structural Matrix Analysis Principle and Program Design*. Chengdu: Southwest Jiaotong University Press.

Xu, Y., Li, Q., Wu, D., & Chen, Z. (2010). Stress and acceleration analysis of coupled vehicle and long-span bridge systems using the mode superposition method. *Engineering Structures*, *32*(5), 1356–1368.

Yang, S., & Hwang, S. (2016). Train-track-bridge interaction by coupling direct stiffness method and mode superposition method. *Journal of Bridge Engineering*, *21*(10). doi: 10.1061/(ASCE)BE.1943-5592.0000852.

Zhai, W. (2015). *Vehicle-track coupling dynamics*. Beijing: Science Press.

Zhang, J., Tan, S., & Wu, C. (2012). A precise integration method for vehicle-track nonlinear coupling and its application. *Journal of Vibration and Shock*, *31*(8), 5–10.

Zhang, X., Shan, Y., & Yang, X. (2017). Effect of bridge-pier differential settlement on the dynamic response of a high-speed railway train-track-bridge system. *Mathematical Problems in Engineering*, *2017*(7), 1–13.

Zhao, G., & Liu, Y. (2020). Mechanism analysis of delamination of CRTS II slab ballastless track structure. *Journal of the China Railway Society*, *42*(7), 117–126.

Zhu, Z., Gong, W., Zhang, L., Yu, Z., & Cai, C. (2018). An efficient hybrid algorithm for dynamic analysis of train-track- bridge coupled system based on separation iterative method and coupled time-varying method. *China Railway Science*, *39*(1), 66–74.

Corresponding author
Mangmang Gao can be contacted at: gaomang@263.net